Kinetic Study of Ca(^{1}S) + N_2O and Sr(^{1}S) + N_2O Reactions in the Temperature Ranges of, Respectively, 303−1015 and 303−999 K

Chris Vinckier,* Joëlle Helaers, and Jan Remeysen

Department of Chemistry, K. U. Leuven, Celestijnenlaan 200F, 3001 Heverlee, Belgium

Received: January 11, 1999; In Final Form: May 10, 1999

A kinetic study of the second-order reactions Ca(^{1}S) + $N_2O(X^1\Sigma^+) \xrightarrow{k_{1_{Ca}}}$ CaO + N_2 and Sr(^{1}S) + $N_2O(X^1\Sigma^+) \xrightarrow{k_{1_{Sr}}}$ SrO + N_2 has been carried out in a fast-flow reactor in the temperature ranges of, respectively, 303−1015 and 303−999 K. The alkaline earth metal atoms were thermally generated from the solid metal pellets. Their decays as a function of the added N_2O concentration were followed by means of atomic absorption spectroscopy (AAS) at 422.7 nm for calcium and 460.7 nm for strontium atoms. Both reactions showed a non-Arrhenius behavior that can best be explained by the presence of two reaction product channels, resulting in a rate constant expressed as the sum of two exponential functions: $k_{1_{Ca}} = [(1.9 \pm 1.4) \times 10^{-8}] \exp[(-40.6 \pm 4.7 \text{ kJ mol}^{-1})/(RT)] + [(2.8 \pm 0.7) \times 10^{-10}] \exp[(-14.1 \pm 0.7 \text{ kJ mol}^{-1})/(RT)]$ cm^3 molecule^{-1} s^{-1}; $k_{1_{Sr}} = [(1.1 \pm 0.2) \times 10^{-9}] \exp[(-23.3 \pm 1.3 \text{ kJ mol}^{-1})/(RT)] + [(1.1 \pm 0.1) \times 10^{-10}] \exp[(-8.8 \pm 0.4 \text{ kJ mol}^{-1})/(RT)]$ cm^3 molecule^{-1} s^{-1}. The best fits over the entire temperature range are given by the polynomial expressions $\log k_{1_{Ca}} = -30.12 + 9.78(\log T) - 0.99(\log T)^2$ and $\log k_{1_{Sr}} = -26.02 + 8.40(\log T) - 1.02(\log T)^2$. The results will be discussed in view of the literature data on the alkaline earth metal atom + N_2O reactions. The experimentally derived energy barriers will be compared with the calculated values on the basis of the semiempirical configuration interaction theory (SECI). Reasonable good correlations were obtained between the barrier heights of the reaction and the promotion energy of the metals involved.

Introduction

Metal atom/N_2O reactions in the gas phase have recently generated considerable interest. The first application is based on the fact that these reactions are very exothermic, leading to product molecules being formed in an electronic excited state.[1] When the metal oxides fall back to lower lying states, an intense chemiluminescence can occur. In this way such reactions can be suitable candidates for the development of chemical lasers in which the population inversion is obtained by means of a pure chemical reaction.[1,2]

Recently, it has also been mentioned that metal/N_2O reactions in incinerators may reduce the emission of the greenhouse gas N_2O.[3] In addition, the study of metal atom/N_2O reactions allows for the testing of empirical models that correlate the experimental Arrhenius parameters with the physicochemical properties of the reaction partners, such as the ionization energy, the electron affinity, etc.[4−10]

A survey of much of the research work concerning metal atom reaction kinetics carried out during the past years has been amply described in ref 11 and more particularly the alkaline earth metal atom/N_2O reactions.[10] Until now, kinetic data for the Mg(^{1}S) atom reaction with N_2O were obtained by means of quite different techniques[12−14] and a fairly good agreement between the rate constants was observed.

Kinetic measurements of the Ca(^{1}S)/N_2O and Sr(^{1}S)/N_2O reactions, however, are rather scarce. Plane and Nien[15] studied the Ca(^{1}S)/N_2O reaction with time-resolved laser-induced fluorescence (LIF) with pulsed photolysis of CaI_2 as the Ca atom source. These authors observed a non-Arrhenius behavior in the temperature range 250−898 K, and the best expression for the temperature dependence of the rate constant was given by

$$k_{1_{Ca}} = [(9.7 \pm 1.4) \times 10^{-10}] \exp\left(\frac{-24.6 \pm 1.1 \text{ kJ mol}^{-1}}{RT}\right) + [(2.4 \pm 0.3) \times 10^{-11}] \exp\left(\frac{-6.8 \pm 0.3 \text{ kJ mol}^{-1}}{RT}\right) \text{ cm}^3 \text{ molecule}^{-1} \text{ s}^{-1} \quad (1)$$

The Ca(^{1}S)/N_2O reaction was also investigated by Kashireninov et al.[16] who used the diffusion flame technique. They measured a temperature dependence in the range 923−1073 K, resulting in the following expression:

$$k_{1_{Ca}} = [(5.6 \pm 0.5) \times 10^{-11}] \exp\left(\frac{-39.3 \pm 7.5 \text{ kJ mol}^{-1}}{RT}\right) \text{ cm}^3 \text{ molecule}^{-1} \text{ s}^{-1} \quad (2)$$

Clay and Husain[17] also investigated the Ca(^{1}S)/N_2O reaction, using a pulsed photolysis technique as the Ca atom source and time-resolved atomic absorption spectroscopy (AAS) as the detection technique. At one single temperature, i.e., 907 K, the value of $1.8 \pm 0.1 \times 10^{-11}$ cm^3 molecule^{-1} s^{-1} was reported, which is a factor of about 2.5 lower than that calculated from the results of Plane and Nien (eq 1).[15] Products of the Ca/N_2O reaction have been monitored in molecular beam experiments by Jonah et al.[18] and Irvin and Dagdigian.[19] Chemiluminescence of the various electronic excited states $A^1\Sigma^+$ and $A'^1\Pi$ of the CaO product molecule was observed, and an upper limit for the total reaction cross section equal to 86.0 ± 5.5 Å^2 was calculated.

10.1021/jp990133a CCC: $18.00
Published on Web 06/19/1999

Until now, the Sr(^{1}S)/N_2O reaction was only investigated by Kashireninov et al.[16] in the temperature region from 943 to 1073 K by means of their diffusion flame technique, which resulted in the expression

$$k_{1_{Sr}} = [(3.5 \pm 0.3) \times 10^{-11}] \exp\left(\frac{-38.5 \pm 8.4 \text{ kJ mol}^{-1}}{RT}\right) \text{cm}^3 \text{ molecule}^{-1} \text{ s}^{-1} \quad (3)$$

Emission from $A^1\Sigma^+$ and $A'^1\Pi$ of SrO has also been observed in molecular beam experiments[20] with an estimated upper value for the total reaction cross section equal to 45.9 ± 2.9 Å^2.

Kinetic measurements of the Ca(^{1}S)/N_2O and Sr(^{1}S)/N_2O reactions will now be presented, covering the pressure and temperature ranges of 6−12 Torr and 303−1015 K for the Ca(^{1}S)/N_2O reaction and 6−12 Torr and 303−999 K for the Sr(^{1}S)/N_2O reaction. The experiments were carried out in a fast-flow reactor using AAS as the detection technique for the thermally evaporated alkaline earth metal atoms. It will be demonstrated that both reactions show a non-Arrhenius behavior that can in principle be explained in terms of transition-state theory or by assuming the presence of two different reaction paths. Finally, the heights of the activation barriers of the Ca(^{1}S)/N_2O and Sr(^{1}S)/N_2O reactions will be verified in terms of how much they are in line with correlations derived for metal atom/N_2O reactions.[4−10]

Experimental Technique

The experimental setup has been amply described in earlier publications,[13,21,22] and only a brief summary will be presented here. It contains two major parts: a fast-flow reactor under low pressure and an AAS detection technique. The reactor consists of a quartz tube with an internal diameter of 5.7 cm and a length of 100 cm. At the upstream end a sample holder contained metal pellets that were thermally evaporated at 600−700 K by means of a kanthal resistance wire. The alkaline earth metal atoms were transported downstream in the kinetic zone by the carrier gas helium, where they were mixed with an excess of N_2O.

In the pressure range from 6 to 12 Torr the flow velocity v_g of the carrier gas helium has a constant value of 320 ± 10 cm s^{-1} at 303 K. Changing the temperature from 303 to 1015 K causes the value of v_g to increase from 320 to 1072 cm s^{-1}. The temperature in the kinetic zone could be varied between 303 and 1000 K by means of an oven, and the temperature was monitored by a chromel−alumel thermocouple. Calcium and strontium atoms were detected by AAS at 422.7 and 460.7 nm, respectively. Assuming that the detection limit corresponds to an absorbance of $A = 0.005$, one can calculate the detection limit for the Ca and Sr atoms by using a formalism explained in an earlier paper:[23] $[\text{Ca(Sr)}] = C_1AL^{-1}T_g^{1/2}$ in which C_1 is a proportionality constant, L the optical path length (5.7 cm), and T_g the gas temperature. With values for $C_1(\text{Ca}) = 0.663 \times 10^{10}$ cm^{-2} K$^{-1/2}$ and $C_1(\text{Sr}) = 0.428 \times 10^{10}$ cm^{-2} K$^{-1/2}$ at 500 K,[24] one can calculate the detection limit for calcium atoms equal to 1.3×10^8 atoms cm^{-3} or 1.12 ppb and for strontium atoms equal to 8.4×10^7 atoms cm^{-3} or 0.72 ppb at 6 Torr and 500 K.

Minimum distances between the metal atom source, the N_2O inlet, and the kinetic zone were maintained to allow for sufficient mixing of the reagents.[21] To derive kinetic data, the decay of the alkaline earth metal atom absorbance was followed as a function of the axial distance z_d along the fast-flow reactor. This was realized by moving the entire reactor assembly along its axis relative to the detection equipment, which remained at a fixed position. Decays of the absorbances as a function of the distance can easily be transformed into decays as a function of the reaction time t using the expression $t = z_d/v_g$. An advantage of this technique is that relative positions of the metal atom source and the N_2O inlet remain constant during the experiments. Reproducible absorbances could be maintained within 10% when the temperature T_s of the metal pellets was stabilized within ±1%.

The gases used in the case of the Ca/N_2O reaction were helium (purity, 99.995%) and mixtures of 1.01 and 9.92% of N_2O in helium (99.995%). The same gases were used for measuring the Sr/N_2O reaction together with a 5.00% mixture of N_2O in helium (99.995%). The calcium pellets (Fluka) and the strontium pellets (Aldrich) respectively had a purity of about 99.5% and 99.0%.

Weighted regressions on all plots were made using the statistical SAS package.[25] The quoted errors σ were the standard deviations.

Results

Determination of the Rate Constants $k_{1_{Ca}}$ and $k_{1_{Sr}}$. The kinetic formalism used in the derivation of the rate constants of the Ca + N_2O and Sr + N_2O reactions has already been described in previous papers.[13,21]

$$\ln A_{\text{Ca(Sr)}} = -\left\{\frac{k_{1_{\text{Ca(Sr)}}}[N_2O]}{\eta} + \frac{7.34D_{\text{Ca(Sr)/He}}}{2r^2}\right\}t + B \quad (4)$$

in which $\ln A_{\text{Ca(Sr)}}$ is the natural logarithm of the calcium or strontium absorbance, η a correction factor depending on the flow characteristics, $D_{\text{Ca(Sr)/He}}$ the binary diffusion coefficients of the Ca and Sr atoms in the carrier gas helium, r the reactor radius, t the reaction time, and B an integration constant. The correction factor η is related to the flow characteristics, and the determination of its magnitude has been amply discussed elsewhere.[26] The use of eq 4 for obtaining kinetic parameters has been well-illustrated in our earlier work[13,27] and will only briefly be summarized here. The values of $k_{1_{\text{Ca(Sr)}}}$ were determined by following first $\ln A_{\text{Ca(Sr)}}$ as a function of the reaction time t with various amounts of N_2O added. A weighted linear regression of $\ln A_{\text{Ca(Sr)}}$ versus t is carried out taking into account a statistical error for $\ln A_{\text{Ca(Sr)}}$, which on average varies between 9.3 and 20.0% going from the highest to the lowest value of $\ln A_{\text{Ca(Sr)}}$.

As an example, Figure 1 shows the pseudo-first-order decays of Ca(^{1}S) atoms as a function of the reaction time t at a temperature $T_g = 303$ K and a pressure P_r of 8 Torr for various initial N_2O concentrations. For the Sr/N_2O reaction similar pseudo-first-order decays were obtained. In the next step the slopes S of these lines are plotted versus the added $[N_2O]$ and a weighted linear regression results in a straight line with a slope directly equal to $k_{1_{\text{Ca(Sr)}}}/\eta$ as is illustrated in Figures 2 and 3 for three different temperatures: 303, 601, and 871 K for the Ca/N_2O reaction and 303, 595, and 999 K for the Sr/N_2O reaction.

In some cases the magnitude of the intercept of these graphs is larger than twice its standard deviation, which implies that plug−flow conditions do not prevail. In these cases the factor η is set equal to 1.3 with an associated systematic error of 10%.[26] In other cases the magnitude of the intercept is about equal to $7.34D_{\text{Ca(Sr)/He}}/(2r^2)$ and a correction factor of 1.6 will be used. The uncertainties σ_S and σ_k for the calculated values of the slope S and the rate constants $k_{1_{\text{Ca(Sr)}}}$ are calculated by combining the uncertainties of several variables such as the temperature, flow velocity, and total pressure as well as of the dimension of the

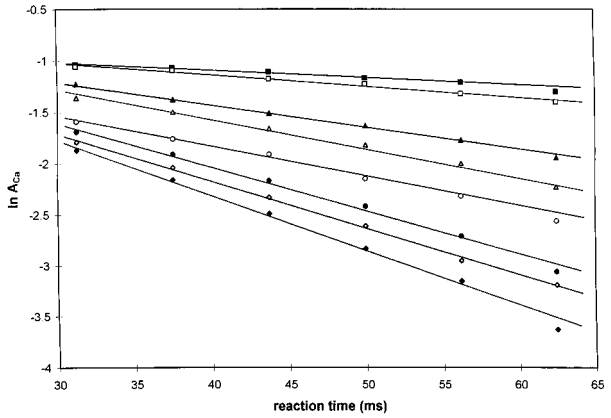

Figure 1. Natural logarithm of the Ca atom absorbance as a function of the reaction time t at various amounts of added N_2O. The experimental conditions are the following: $T_g = 303$ K; $P_r = 8$ Torr; He as carrier gas; [N_2O] (■) 0, (□) 0, (▲) 19.2, (△) 27.6, (○) 36.0, (●) 45.1, (◇) 54.2, and (◆) 62.7 expressed in units of 10^{12} molecules cm^{-3}.

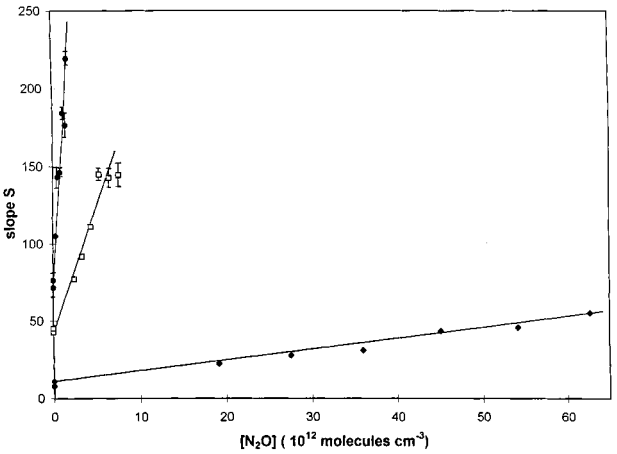

Figure 2. Slopes S from Figure 1 as a function of the added N_2O concentration. The experimental conditions are the following: $P_r = 8$ Torr; He as carrier gas; $T_g = 303$ K (◆), 601 K (□) and 871 K (●).

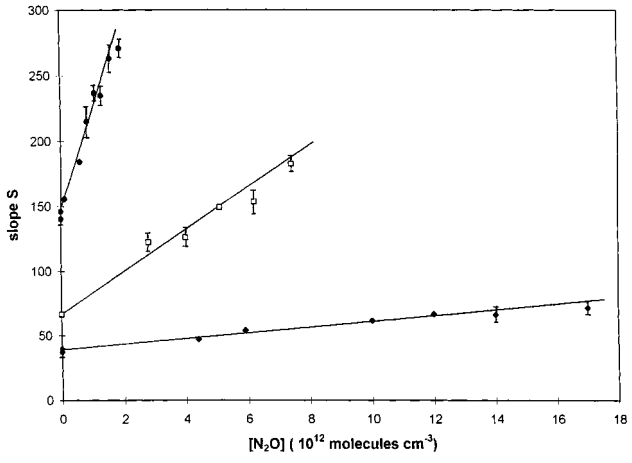

Figure 3. Slopes S from the plot of ln A_{Sr} vs t as a function of the added N_2O concentration. The experimental conditions are the following: $P_r = 8$ Torr; He as carrier gas; $T_g = 303$ K (◆), 595 K (□), and 999 K (●).

reactor radius according to the method explained in detail by Howard.[28] When the correction factor 1.3 was used, a systematic error of 10% was taken into account, resulting in the total standard deviation σ_k. Finally, the observed slopes in Figures 2 and 3 need to be multiplied by η to obtain the correct second-order rate constants $k_{1_{Ca(Sr)}}$. In the examples mentioned above,

TABLE 1: Influence of the Pressure P_r (a) and the Initial Absorbances A^i_{Ca} and A^i_{Sr} (b) on the Second-Order Rate Constants $k_{1_{Ca(Sr)}}$

(a) Pressure Effect

T_g (K)	P_r (Torr)	$k_{1_{Ca}}$ ($\times 10^{-12}$ cm^3 molecule^{-1} s^{-1})	T_g (K)	P_r (Torr)	$k_{1_{Sr}}$ ($\times 10^{-12}$ cm^3 molecule^{-1} s^{-1})
303	6	1.0 ± 0.1	303	6	3.7 ± 0.1
303	6	0.9 ± 0.1	303	8	3.4 ± 0.2
303	8	1.1 ± 0.2	303	9	3.7 ± 0.2
303	8	0.9 ± 0.1	303	11	3.5 ± 0.3
303	10	1.1 ± 0.1	303	12	3.1 ± 0.2
303	12	1.2 ± 0.2			

(b) Effect of Initial Absorbance

T_g (K)	A^i_{Ca}	$k_{1_{Ca}}$ ($\times 10^{-12}$ cm^3 molecule^{-1} s^{-1})	T_g (K)	A^i_{Sr}	$k_{1_{Sr}}$ ($\times 10^{-12}$ cm^3 molecule^{-1} s^{-1})
303	0.09	1.0 ± 0.1	303	0.16	3.7 ± 0.1
303	0.49	1.1 ± 0.2	303	0.35	3.5 ± 0.3
545	0.26	19.0 ± 3.0	599	0.14	25.4 ± 3.7
545	0.56	22.0 ± 3.0	599	0.29	21.5 ± 3.2
647	0.06	32.0 ± 6.0	948	0.10	89.3 ± 11.1
647	0.39	32.0 ± 6.0	948	0.22	91.7 ± 5.1

at 8 Torr of He, second-order rate constants $k_{1_{Ca}} = 1.1 \pm 0.2$, 21.0 ± 3.0, and 110.0 ± 20.0 in units of 10^{-12} cm^3 molecule^{-1} s^{-1} are derived at 303, 601, and 871 K, respectively. In the case of the Sr/N_2O reaction, values for $k_{1_{Sr}}$ equal to 3.4 ± 0.2, 25.2 ± 1.3, and 113.8 ± 6.0 in units of 10^{-12} cm^3 molecule^{-1} s^{-1} are derived at 303, 595, and 999 K, respectively.

To confirm the second-order behavior of both reactions, the pressure dependence of the rate constants $k_{1_{Ca(Sr)}}$ was examined. Table 1 shows that at 303 K $k_{1_{Ca(Sr)}}$ is independent of the pressure, since no systematic trends can be noticed in the pressure range between 6 and 12 Torr. This implies that at the lowest temperature third-order reactions do not contribute to the metal atom decays, and in this case, we do not expect an effect of such reactions at higher temperatures.

These experiments also confirm that hydrodynamic effects, since there is the mixing of the reagents or the wall loss of Ca or Sr atoms, have no influence on the derived values of the rate constants.

The effect of the initial alkaline earth metal atom concentration on the value of $k_{1_{Ca(Sr)}}$ has also been checked. For this purpose, A^i_{Ca} and A^i_{Sr} were varied by a factor of, respectively, 2−6 and 2 at various temperatures. Table 1 shows that in both cases a change of the initial absorbance has no systematic effect on $k_{1_{Ca(Sr)}}$. This proves that, as expected, at these low initial metal atom concentrations, mutual reactions between the metal atoms or consecutive reaction steps involving these metal atoms are unimportant.

Temperature Dependence of $k_{1_{Ca}}$ and $k_{1_{Sr}}$. The experimental conditions together with all the values of $k_{1_{Ca}}$ and $k_{1_{Sr}}$ determined in the temperature ranges of, respectively, 303−1015 and 303−999 K are listed in Table 2.

The values of $k_{1_{Ca(Sr)}}$ from Table 2 are shown in an Arrhenius plot in Figures 4 and 5.

Both reactions show a non-Arrhenius behavior in view of the upward curvatures, which become pronounced at temperatures above 500 K.

According to transition-state theory, a non-Arrhenius behavior can be accounted for by introducing a temperature-dependent preexponential factor resulting in an expression for the reaction rate constant $k(T) = AT^n \exp[-E/(RT)]$.[29] For N_2O reactions a temperature dependence T^n can be explained by taking into

TABLE 2: Rate Constants $k_{1_{Ca}}$ and $k_{1_{Sr}}$ of the Reactions Ca(^{1}S) + N_2O and Sr(^{1}S) + N_2O as a Function of the Gas Temperature T_g[a]

T_g (K)	P_r (Torr)	A^i_{Ca}	η	$k_{1_{Ca}}$ ($\times 10^{-12}$ cm^3 molecule^{-1} s^{-1})	T_g (K)	P_r (Torr)	A^i_{Sr}	η	$k_{1_{Sr}}$ ($\times 10^{-12}$ cm^3 molecule^{-1} s^{-1})
303	6	0.09	1.6	1.0 ± 0.1	303	6	0.16	1.6	3.7 ± 0.1
303	6	0.21	1.3	0.9 ± 0.1	303	8	0.23	1.6	3.4 ± 0.2
303	8	0.49	1.3	1.1 ± 0.2	303	9	0.31	1.6	3.7 ± 0.2
303	8	0.35	1.3	0.9 ± 0.1	303	11	0.35	1.6	3.5 ± 0.3
303	10	0.25	1.6	1.1 ± 0.1	303	12	0.18	1.6	3.1 ± 0.2
303	12	0.39	1.3	1.2 ± 0.2	349	8	0.26	1.3	4.3 ± 0.7
328	10	0.46	1.3	2.1 ± 0.3	369	8	0.21	1.6	6.2 ± 0.1
354	8	0.57	1.3	2.2 ± 0.4	400	8	0.20	1.3	7.0 ± 0.9
382	10	0.26	1.3	3.3 ± 0.4	408	8	0.28	1.6	9.9 ± 0.2
415	8	0.35	1.3	5.1 ± 0.8	408	8	0.12	1.6	8.9 ± 0.7
437	10	0.21	1.3	7.1 ± 0.8	422	8	0.36	1.3	8.8 ± 1.3
484	8	0.33	1.3	7.3 ± 0.8	445	8	0.37	1.3	10.2 ± 1.4
501	8	0.15	1.3	10.0 ± 2.0	446	8	0.19	1.3	10.1 ± 1.6
545	10	0.56	1.3	22.0 ± 3.0	502	8	0.22	1.6	18.4 ± 0.9
545	10	0.26	1.3	19.0 ± 3.0	541	8	0.18	1.6	24.0 ± 1.3
601	8	0.36	1.3	21.0 ± 3.0	595	6	0.10	1.6	30.7 ± 3.0
647	8	0.39	1.3	32.0 ± 6.0	595	8	0.48	1.6	25.2 ± 1.3
647	8	0.06	1.3	32.0 ± 6.0	595	9	0.12	1.6	33.4 ± 1.1
691	10	0.27	1.3	43.0 ± 9.0	595	11	0.16	1.6	34.7 ± 1.4
744	10	0.47	1.3	52.0 ± 10.0	595	12	0.29	1.6	27.9 ± 2.0
780	8	0.27	1.3	62.0 ± 15.0	599	8	0.29	1.3	21.5 ± 3.2
831	10	0.58	1.3	89.0 ± 13.0	599	8	0.14	1.3	25.4 ± 3.7
831	10	0.14	1.3	110.0 ± 20.0	625	8	0.20	1.6	32.4 ± 0.8
871	8	0.38	1.3	110.0 ± 20.0	654	8	0.19	1.6	31.8 ± 1.4
917	10	0.21	1.3	120.0 ± 20.0	692	8	0.15	1.3	34.9 ± 4.5
1015	10	0.21	1.6	250.0 ± 50.0	744	8	0.14	1.3	38.9 ± 5.1
					790	8	0.18	1.3	44.8 ± 6.6
					848	8	0.12	1.3	60.0 ± 8.9
					869	8	0.16	1.3	47.8 ± 6.4
					939	8	0.25	1.3	72.6 ± 10.8
					948	8	0.10	1.6	89.3 ± 11.1
					948	8	0.22	1.6	91.7 ± 5.1
					991	8	0.24	1.6	110.0 ± 3.7
					999	8	0.52	1.6	113.8 ± 6.0

[a] P_r is the reactor pressure and $A^i_{Ca(Sr)}$ is the initial absorbance. The flow velocity v_g of the carrier gas helium increases from 320 to 1072 cm s^{-1} when going from 303 to 1015 K.

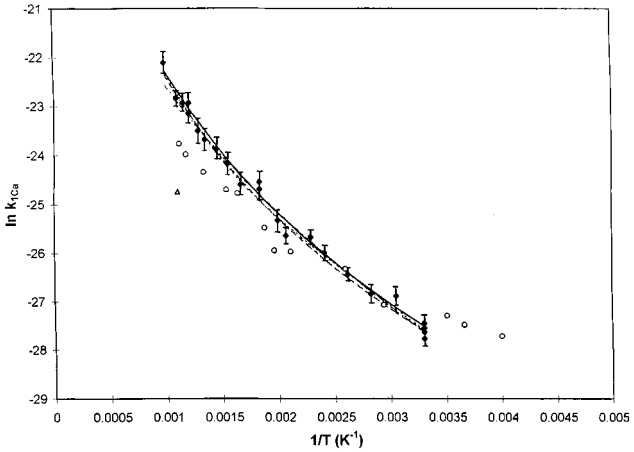

Figure 4. Plot of ln $k_{1_{Ca}}$ vs $1/T$ according to the model of two separate reaction channels (- - -) (eq 6), the transition-state theory fit with a temperature dependence $T^{3.6}$ (— — —) (eq 5), and the polynomial fit (—) (eq 8). Also shown are the results of Plane and Nien[15] (○) and of Clay and Husain[17] (△).

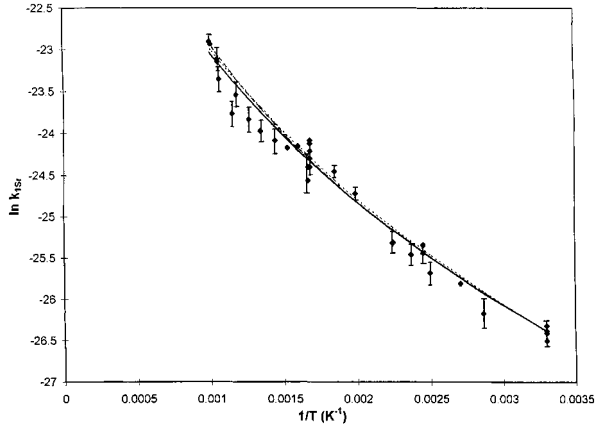

Figure 5. Plot of ln $k_{1_{Sr}}$ vs $1/T$ according to the transition-state theory fit $T^{2.2}$ (— — —), the fit based on the presence of two separate reaction channels (- - -) (eq 7), and the polynomial fit (—) (eq 9).

account the vibrational excitation of the N_2O molecule at high temperatures because then the ν_2 bending vibration levels of the ground-state N_2O become more strongly populated. At 1000 K this bending vibration ν_2 can be excited to a vibrational quantum number of 5 ($v = 5$). A more extensive discussion of the role of vibrationally excited N_2O can be found in refs 15, 30, and 31 and references therein. When N_2O in its linear ground state must accept an electron, the endothermic vertical electron affinity of the formed linear N_2O^- anion requires a considerable energy barrier. However, in the bended configuration the adiabatic electron affinity becomes positive, which strongly increases the probability for an electron transfer. As a result, the vibrational excitation of N_2O up to $v = 5$ at a high temperature enhances the reaction rate and could explain the observed non-Arrhenius behavior of the Ca/N_2O and Sr/N_2O reactions.

The values of A, n, and E can be determined by means of a weighted nonlinear regression using the SAS software.[25] For

TABLE 3: Reaction Enthalpy ΔH_R of the Reactions of Ca and Sr in Their Ground States with N_2O, Leading to Various Electronic Excited States of the Corresponding Metal Oxide[37]

	possible states of the metal oxide	ΔH_R (kJ mol^{-1})
spin-allowed	$Ca(^1S) + N_2O \rightarrow CaO(X^1\Sigma^+) + N_2$	−216.0
	$Ca(^1S) + N_2O \rightarrow CaO(A'^1\Pi) + N_2$	−113.0
	$Ca(^1S) + N_2O \rightarrow CaO(A^1\Sigma^+) + N_2$	−77.8
spin-forbidden	$Ca(^1S) + N_2O \rightarrow CaO(a^3\Pi) + N_2$	−117.6
	$Ca(^1S) + N_2O \rightarrow CaO(^3\Sigma^+) + N_2$	−96.4
spin-allowed	$Sr(^1S) + N_2O \rightarrow SrO(X^1\Sigma^+) + N_2$	−260.0
	$Sr(^1S) + N_2O \rightarrow SrO(A'^1\Pi) + N_2$	−142.8
	$Sr(^1S) + N_2O \rightarrow SrO(A^1\Sigma^+) + N_2$	−130.0
spin-forbidden	$Sr(^1S) + N_2O \rightarrow SrO(a^3\Pi) + N_2$	−152.0
	$Sr(^1S) + N_2O \rightarrow SrO(^3\Sigma^+) + N_2$	−164.3

the Ca + N_2O reaction the value of n was kept fixed and was allowed to vary with increments of 0.1 between 1.5 and 4.0. A minimum in the sum of squares of the residuals was obtained at $n = 3.6$, resulting in the following expression:

$$k_{1_{Ca}} = [(4.4 \pm 0.5) \times 10^{-21}]T^{3.6} \exp\left(\frac{-3.3 \pm 0.3 \text{ kJ mol}^{-1}}{RT}\right) \text{ cm}^3 \text{ molecule}^{-1} \text{ s}^{-1} \quad (5)$$

This fit is shown in Figure 4, and a reasonable agreement between calculated and experimental rate constants is obtained. However, the value of 3.6 for the temperature exponent is too high and cannot be explained on the basis of the transition-state theory. Indeed, Cohen[32] calculated possible values for n, taking into account the geometry of the activated complex as well as anharmonic oscillations. He arrived at an upper value of $n = 2.2$. When this value was selected and kept fixed, the resulting expression led to a fit that was nearly the same as for eq 5 and is therefore not shown in Figure 4.

When the same procedure was applied for the Sr/N_2O reaction no minimum in the sum of squares of the residuals could be achieved in the range of n values between 1.0 and 2.9. Calculations with values for n higher than 2.9 were useless because the activation barrier even became negative. Therefore, the value for n was arbitrarily set at 2.2.[32] From Figure 5 one sees that for the Sr/N_2O reaction the $T^{2.2}$ fit also represents the experimental data quite well, so one may conclude that the data are not sensitive to the value of the temperature exponent n. From the above it is clear that although the curvature in the Arrhenius plots might be explained on the basis of the transition-state theory, our results do not allow us to determine the value of the temperature exponent n or the magnitude of the energy barrier.

An attractive alternative for explaining the non-Arrhenius behavior is the existence of two reaction paths with different energy barriers, as has been experimentally determined for the Mg/N_2O reaction, i.e., 28.8 and 38.4 kJ mol^{-1}.[33] An analogous mechanism can also be proposed for the Ca/N_2O and Sr/N_2O reactions. According to path 1, the Ca and Sr atoms in their ground states (^1S) react with N_2O, forming respectively CaO($X^1\Sigma^+$) and SrO($X^1\Sigma^+$) and respecting the "conservation of total spin" principle. But in addition, the Ca(Sr)/N_2O reactions can also lead to the formation of the triplet states of the reaction products CaO($a^3\Pi$) and SrO($a^3\Pi$), but these reactions are nonadiabatic with respect to the spin (path 2). As an illustration, Table 3 shows the reaction enthalpy ΔH_R of the reactions of Ca and Sr in their ground states with N_2O, leading to various electronic states of the corresponding metal oxide.

Table 3 indicates that both singlet and triplet metal oxide products are accessible, where their formation will imply a different activation energy. The observed rate constant can thus be written as a sum of two exponential functions: $A_1 \exp[-E_1/(RT)] + A_2 \exp[-E_2/(RT)]$. To derive the four parameters A_1, E_1, A_2, and E_2, a special procedure was followed. In the first approximation the low-temperature data in the Arrhenius plot were considered as linear. The upper temperature limit was arbitrarily set at 500 K, and values for A_2 and E_2 in the low-temperature range were calculated. In the next step all the rate constants over the entire temperature range from 303 to approximately 1000 K were fitted with the values of the parameters A_2 and E_2 kept fixed so that only A_1 and E_1 need to be determined. Then all the rate constants were fitted again, but now the parameters A_1 and E_1 were kept fixed and only the values of A_2 and E_2 needed to be calculated again. With these newly obtained values of A_2 and E_2, the values of A_1 and E_1 were recalculated. This oscillation procedure was continued until the lowest value in the sum of squares of the residuals was obtained, giving the following expressions:

$$k_{1_{Ca}} = [(1.9 \pm 1.4) \times 10^{-8}] \exp\left(\frac{-40.6 \pm 4.7 \text{ kJ mol}^{-1}}{RT}\right) + [(2.8 \pm 0.7) \times 10^{-10}] \exp\left(\frac{-14.1 \pm 0.7 \text{ kJ mol}^{-1}}{RT}\right) \text{ cm}^3 \text{ molecule}^{-1} \text{ s}^{-1} \quad (6)$$

$$k_{1_{Sr}} = [(1.1 \pm 0.2) \times 10^{-9}] \exp\left(\frac{-23.3 \pm 1.3 \text{ kJ mol}^{-1}}{RT}\right) + [(1.1 \pm 0.1) \times 10^{-10}] \exp\left(\frac{-8.8 \pm 0.4 \text{ kJ mol}^{-1}}{RT}\right) \text{ cm}^3 \text{ molecule}^{-1} \text{ s}^{-1} \quad (7)$$

It should be pointed out here that the choice of the starting values of the parameters A_1, E_1, A_2, and E_2 within reasonable limits had no influence on the final values of the Arrhenius parameters obtained. Furthermore, the choice of the upper temperature where the first values of A_2 and E_2 were calculated is not critical. If instead of 500 K the linear part for the first iteration was set at 650 K, final values for A_1, E_1, A_2, and E_2 were obtained within the error range of those shown in eqs 6 and 7. In Figures 4 and 5 one sees that both expressions fit the experimental data for the Ca/N_2O and Sr/N_2O reactions fairly well.

From the above one sees that both the transition-state theory and the two-path mechanism fit the experimental results fairly well (see Figures 4 and 5). One must conclude that on the basis of the kinetic data derived in the temperature range covered in this work, no final decision can be made about which of the two explanations prevails. One way to clarify this problem is by experimentally determining the magnitude of the energy barriers. By means of their molecular beam technique experiments Costes et al.[33] measured two translational energy barriers E_1 and E_2 to be respectively 38.4 and 28.8 kJ mol^{-1} for the analogous Mg/N_2O reaction. In this way the two-channel mechanism was clearly established for the Mg/N_2O reaction, but unfortunately, no such data are available for the Ca/N_2O and Sr/N_2O reactions. Taking into account that on the basis of the transition state, no values for n, A, or E could be derived that are physically meaningful, the kinetic expressions based on the occurrence of two different reaction paths (eqs 6 and 7) will be preferred. A second advantage of eqs 6 and 7 is that they represent the low- and high-temperature dependences of the Ca/N_2O and Sr/N_2O reactions as two separate terms, which

in principle allows us to fit the values of the rate constants in a better way.[15]

Finally, the experimental data for both reactions were also fitted to the second-degree polynomial expressions:

$$\log k_{1_{Ca}} = -30.12 + 9.78(\log T) - 0.99(\log T)^2 \quad (8)$$

$$\log k_{1_{Sr}} = -26.02 + 8.40(\log T) - 1.02(\log T)^2 \quad (9)$$

These polynomial fits are excellent representations of the experimental values (see Figures 4 and 5), but they do not have any kinetic meaning.

Discussion

Comparison with Other Experimental Data. As already mentioned before Plane and Nien[15] used a time-resolved LIF flash photolysis technique for studying the Ca/N_2O reaction. They also observed a clear non-Arrhenius behavior, and they derived eq 1 for describing the temperature dependence of $k_{1_{Ca}}$ between 250 and 898 K. Apparently, a large discrepancy exists between the values of their Arrhenius parameters A_1, E_1, A_2, and E_2 in eq 1 and our values in eq 6. But when the values of the rate constants were plotted, the deviation is much less pronounced as is also illustrated in Figure 4. While the agreement between the values obtained by both techniques at temperatures below 500 K is fairly good, our values are a factor of 1.4 to 3.3 higher at temperatures above 500 K. The reason for this discrepancy is not at all clear, especially since both techniques showed a very good agreement for the Mg/N_2O reaction.[12,13] It is also checked whether the statistical treatment of the data could be the reason for quite different values for the Arrhenius parameters. When we applied our oscillation procedure to the experimental data of Plane and Nien,[15] we obtained the expression $k_{1_{Ca}} = [(9.6 \pm 3.2) \times 10^{-10}] \exp[-24.4 \pm 2.0$ kJ mol^{-1}/(RT)] + [$(2.3 \pm 0.5) \times 10^{-11}$] exp[$-6.7 \pm 0.5$ kJ mol^{-1}/(RT)] cm^3 molecule^{-1} s^{-1}. One sees that the resulting values for A_1, E_1, A_2, and E_2 perfectly fall within the ranges given in eq 1. This proves that the statistical treatment applied by Plane and Nien,[15] which was certainly different from ours, cannot explain the difference between the Arrhenius parameters derived in both studies.

An interesting feature of the Arrhenius expressions 6 and 7 is the high values of the preexponential factor A_1, which have also been observed in the Li/N_2O and K/N_2O reactions.[10] This must be seen in terms of the electron jump mechanism,[34] in which an electron from the metal atom will be transferred to the N_2O molecule to form N_2O^-. This mechanism might prevail at high temperatures, since Chantry observed a substantial increase of the dissociative attachment rate of the reaction $N_2O + e^- \rightarrow N_2 + O^-$ with a factor of 1000 between 350 and 1000 K.[30]

The only other expressions to compare with are eqs 2 and 3, obtained by means of the diffusion flame technique.[16] However, at the highest temperatures covered in our work eqs 2 and 3 result in values for $k_{1_{Ca}}$ and $k_{1_{Sr}}$, which are respectively about a factor of 400 and 300 lower than our values. It needs to be pointed out that the use of the diffusion flame technique[16] strongly complicates the interpretation of the results through both the complexity of the reaction mechanism as well as the presence of temperature and concentration gradients.

From our measurements one can calculate the cross sections for the Ca(Sr)/N_2O reactions at room temperature as well as at the highest experimental temperature. For the Ca/N_2O reaction these values are equal to 0.2 Å^2 at 303 K and 20.5 Å^2 at 1015 K. For the Sr/N_2O reaction cross sections of 0.7 Å^2 at 303 K and 12.4 Å^2 at 999 K were obtained. These cross sections can be compared with the values derived from molecular beam experiments, i.e., 86.0 Å^2 for the Ca/N_2O reaction and 45.9 Å^2 for the Sr/N_2O reaction.[19,20] The authors commented that these large cross sections are upper limits that might be due to a significant elastic scattering contribution to Ca and Sr loss in their molecular beam studies.

Correlation between Experimental Arrhenius Parameters and Physicochemical Properties of the Reactants. The dynamical aspects of the alkaline earth metal/N_2O reactions have already been discussed extensively in the literature,[6,10,12,15,31] and only some essential features will be repeated here. As already mentioned, a possible explanation for the observed non-Arrhenius behavior is related to the occurrence of two reaction paths. First, an adiabatic reaction path under C_s symmetry along the lowest ^{1}A′ potential energy surface will yield the metal oxide in its ground state $X^1\Sigma^+$. This reaction is spin-allowed but is characterized by a high activation energy; E_1 is equal to 40.6 and 23.3 kJ mol^{-1} for the Ca/N_2O and Sr/N_2O reactions, respectively. Ab initio calculations have shown that, for example, the Mg/N_2O reaction proceeds through an intermediate charge-transfer complex $Mg^+(^2S)N_2O^-(^2A')$ located on the ^{1}A′ surface 59.7 kJ mol^{-1} below the reactants.[31] Owing to the poor overlap between the s orbitals of the metal and the 3π orbital of N_2O, the possibility for charge transfer is rather small, resulting in a relatively high energy barrier. If, however, open-shell ^{1}D or ^{1}P states of the metal atom become accessible, the orbital overlap will strongly be enhanced and the height of the energy barrier will be reduced. For the Ca and Sr atoms the lowest excited ^{1}D states are lying respectively 260.9 and 240.6 kJ mol^{-1} above the ground state,[35] in qualitative agreement with the lower Arrhenius activation energy of 23.3 kJ mol^{-1} for the Sr/N_2O reaction (eq 7) compared to 40.6 kJ mol^{-1} for the Ca/N_2O reaction (eq 6).

In addition, a nonadiabatic transition along the ^{3}A′ surface can lead to the formation of metal oxide products in the triplet state ($a^3\Pi$). In eqs 6 and 7 this path is characterized by the energy barrier E_2 equal to 14.1 and 8.8 kJ mol^{-1} for the Ca/N_2O and Sr/N_2O reactions, respectively. The fact that the barrier height for this nonadiabatic reaction path is lower than for the adiabatic reaction can simply be explained by the fact that the accessible ^{3}P state of the metal atom is situated at a lower energy level than the ^{1}D or ^{1}P states.[10] Concerning the relative magnitude of the preexponential factors A_1 and A_2 in eqs 6 and 7, one knows that a nonadiabatic transition, in this case from the ^{1}A′ to the ^{3}A′ potential energy surface in the entrance channel, reduces the reaction probability. Since this probability is related to the value of A_2, it can be calculated as the ratio $A_2/(A_1 + A_2)$. From eqs 6 and 7 values of 0.015 for the Ca/N_2O and 0.091 for the Sr/N_2O reaction were derived. One can conclude that the spin-forbidden reaction path, leading to the formation of CaO($a^3\Pi$) and SrO($a^3\Pi$), will dominate in the low-temperature region. Starting at about 500 K, the spin-allowed channel, forming the reaction products CaO($X^1\Sigma^+$) and SrO($X^1\Sigma^+$), will compete and will even become the dominating reaction path when the temperature is further increased.

On the basis of the considerations made above, Futerko and Fontijn developed a semiempirical model for calculating the barrier heights for a large number of metal/N_2O reactions.[4] Later on, the method was refined for the s^2 metals and especially the contributions from spin-forbidden channels have been taken into account.[6] Reasonable good fits between the calculated and experimental rate constants were obtained for the Mg, Ca, and

TABLE 4: Comparison between the Calculated $E_{1,2}$(calc) and the Experimental Activation Barriers $E_{1,2}$(exp) for the Alkaline Earth Metal Atom/N_2O Reactions[a]

metal atom	E_1(calc) (kJ mol^{-1})	E_1(exp) (kJ mol^{-1})	E_2(calc) (kJ mol^{-1})	E_2(exp) (kJ mol^{-1})
Mg	43.8 (6)	37.2 (12)	26.3 (6)	28.8 (33)
		41.6 (13)		
		28.5 (14)		
		44.0 (16)		
		38.4 (33)		
Ca	15.2 (6)	22.6 (15)	6.8 (6)	4.9 (15)
		38.3 (our work)		11.8 (our work)
		35.2 (16)		
Sr	0.0 (4)	21.0 (our work)	− (4)	6.5 (our work)
		34.3 (16)		
Ba	16.3 (6)	18.5 (16)	2.9 (6)	3.8 (36)

[a] The references are indicated in parentheses.

Ba/N_2O reactions with calculated values that are slightly lower than the experimental ones for the Ba/N_2O and Ca/N_2O reactions at temperatures above 500 K. In Table 4 the calculated values E_1(calc) for the spin-allowed channels and E_2(calc) for the spin-forbidden channels are being compared with the experimentally determined energy barriers E_1(exp) and E_2(exp). Despite the problems for extracting kinetic parameters by means of the diffusion flame technique, values for the activation barriers derived with this technique are also given in Table 4. Indeed, it has already been pointed out by several authors that this technique allows us to determine quite well the temperature dependence of the rate constant but not the preexponential factor.[12−15]

The experimental activation barriers $E_{1,2}$(exp) were derived by converting the experimentally determined Arrhenius activation energy E_a by means of the relationship $E_{1,2}(\text{exp}) = E_a - nR(T_1T_2)^{0.5}$, in which T_1 and T_2 are the limits of the temperature range over which the experimental rate constant is considered and n was set equal to 0.5, which led to the best agreement with experimental results.[4]

From Table 4 one sees that a good agreement is obtained for the Mg/N_2O reaction while for the Ca and Sr/N_2O reactions the calculated barriers are systematically lower than the experimental values. For the Ba/N_2O reaction, two experimental values of the energy barrier were determined.[16,36] One can note that the experimental energy barrier of 3.8 kJ mol^{-1} [36] might correspond to a spin-forbidden reaction channel, while the value of 18.5 kJ mol^{-1} [16] might be assigned to a spin-allowed reaction path. In this case the agreement with the calculated energy barriers E_1(calc) and E_2(calc) of 16.3 and 2.9 kJ mol^{-1}, respectively, is quite good.

It should be remembered that the semiempirical calculations were based on the assumption that the transition state is composed of three hypothetical resonating structures. The first one is the result of a covalent interaction between the oxygen atom in the N_2O molecule and the metal atom in which the bonding orbital of the metal has s character. The second structure is related to a covalent interaction between the O atom and the metal atom, but in this case the bonding orbital of the metal has p character, originating from the first spin-allowed electronic transition. The third structure is ionic and results from the interaction between the negatively charged N_2O^- ion and the partially charged metal ion.[4] In view of the foregoing it was logical to try out a correlation between the experimentally determined energy barriers and the so-called promotion energy defined here as the sum of the ionization energy IE and the excitation energy of the lowest-lying singlet state (1) or triplet state (3) of the metal atom.[4] The formation of metal oxides in the triplet state requires another transition state to be considered in which the interaction between the lowest-lying triplet state of the metal atom and the N_2O molecule must be taken into account.

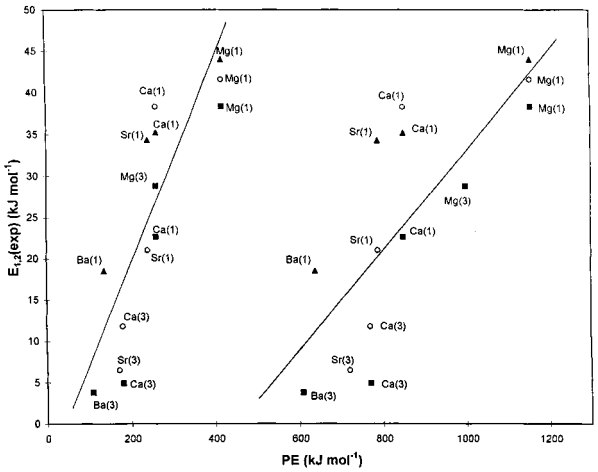

Figure 6. Correlation between the experimental activation barriers $E_{1,2}$(exp) and the promotion energy PE for several alkaline earth metal atom/N_2O reactions: results of Plane[10] (■), Kashireninov et al.[16] (▲), and this work (○). For values for the experimental barriers $E_{1,2}$(exp), see Table 4. The promotion energy PE is defined in two ways. On the left side of the figure PE is set equal to the excitation energy of the lowest-lying triplet state, labeled (3), or the lowest-lying excited singlet state, labeled (1), of the metal atom. On the right side of the figure $E_{1,2}$(exp) is plotted as a function of the sum of the excitation energy and the ionization energy IE of the metal atom.

This correlation is shown on the right side of Figure 6 where the experimental value of the energy barrier for the alkaline earth metal atom/N_2O reaction is plotted as a function of the promotion energy.

Plane[10] also tried another correlation in which the promotion energy was defined as the excitation energy to the lowest-lying triplet or singlet state with omission of the ionization energy. As one can see at the left side of Figure 6, the last type of correlation seems to be somewhat better, which might indicate that the charge-transfer path through avoided crossings with the ionic potential energy surface is less important.[10] In conclusion one is allowed to state that, except for our measured energy barrier E_1(exp) of the Ca/N_2O reaction, these types of correlation are a very valuable tool for estimating kinetic parameters of metal atom/N_2O reactions. Of course, it must be taken into account that each type of electron configuration, e.g., s^1, s^2, s^2p^1, or s^2p^2 of the metal atom, probably leads to a different relationship.[9] Finally, it should be mentioned that, as the work of Fontijn et al.[8] has shown, these types of correlation are not limited to metal atom/N_2O reactions but can also be extended to various oxidants such as O_2, CO_2, and SO_2 with a large variety of diatomic species.

Acknowledgment. We thank the Fund for Joint Basic Research (FKFO), Brussels, Belgium, for a research grant. C.V. is a Research Director of the National Fund for Scientific Research (Belgium). J.H. is grateful to the Institute for Science and Technology (IWT) for granting her a doctoral fellowship.

References and Notes

(1) Cool, T. A. *Reaction Dynamics*; Smith, I. W. M., Ed.; Physical Chemistry of Fast Reactions 2; Plenum Press: New York, 1980; p 215.

(2) Herbelin, J. M.; Cohen, N. *J. Quant. Spectrosc. Radiat. Transfer* **1975**, *15*, 731.

(3) Perry, R. A.; Miller, J. A. *Int. J. Chem. Kinet.* **1996**, *28*, 217.

(4) Futerko, P. M.; Fontijn, A. *J. Chem. Phys.* **1991**, *95*, 8065.
(5) Futerko, P. M.; Fontijn, A. *J. Chem. Phys.* **1992**, *97*, 3861.
(6) Futerko, P. M.; Fontijn, A. *J. Chem. Phys.* **1993**, *98*, 7004.
(7) Belyung, D. P.; Futerko, P. M.; Fontijn, A. *J. Chem. Phys.* **1995**, *102*, 1.
(8) Blue, A. S.; Belyung, D. P.; Fontijn, A. *J. Chem. Phys.* **1997**, *107*, 10.
(9) Fontijn, A. *Pure Appl. Chem.* **1998**, *70*, 2, 469.
(10) Plane, J. M. C. *Gas-Phase Metal Reactions*; Fontijn, A., Ed.; Elsevier: Amsterdam, 1992; p 29.
(11) *Gas-Phase Metal Reactions*; Fontijn, A., Ed.; Elsevier: Amsterdam, 1992.
(12) Plane, J. M. C.; Nien, C. F.; Rajasekhar, B. *J. Phys. Chem.* **1992**, *96*, 1296.
(13) Vinckier, C.; Christiaens, P. *J. Phys. Chem.* **1992**, *96*, 2146.
(14) Michels, H. H.; Meinzer, R.; Tripodi, R. *Inst. Phys. Conf. Ser.* **1985**, No. 72, 193.
(15) Plane, J. M. C.; Nien, C. F. *J. Phys. Chem.* **1990**, *94*, 5255.
(16) Kashireninov, O. E.; Manelis, G. B.; Repka, L. F. *Russ. J. Phys. Chem.* **1982**, *56*, 630.
(17) Clay, R. S.; Husain, D. *Combust. Flame* **1991**, *86*, 371.
(18) Jonah, C. D.; Zare, R. N.; Ottinger, Ch. *J. Chem. Phys.* **1972**, *56*, 263.
(19) Irvin, J.; Dagdigian, P. J. *J. Chem. Phys.* **1981**, *74*, 6178.
(20) Cox, J. W.; Dagdigian, P. J. *J. Phys. Chem.* **1982**, *86*, 3738.
(21) Vinckier, C.; Christiaens, C. *J. Phys. Chem.* **1992**, *96*, 8423.
(22) Vinckier, C.; Christiaens, P.; Hendrickx, M. *Gas-Phase Metal Reactions*; Fontijn, A., Ed.; Elsevier: Amsterdam, 1992; p 57.
(23) De Jaegere, S.; Willems, M.; Vinckier, C. *J. Phys. Chem.* **1982**, *86*, 3569.
(24) Brouwers, H. Ph.D. Thesis, Faculty of Science, K. U. Leuven, 1984.
(25) *S.A.S. Statistical Package*; S.A.S. Institute Inc.: Cary, NC, 1989.
(26) Fontijn, A.; Felder, W. *Reactive Intermediates in the Gas-Phase, Generation and Monitoring*; Setser, W., Ed.; Academic Press: New York, 1979; p 59.
(27) Vinckier, C.; Corthouts, J.; De Jaegere, S. *J. Chem. Soc., Faraday Trans. 2* **1988**, *84*, 1951.
(28) Howard, C. J. *J. Phys. Chem.* **1979**, *83*, 3.
(29) Fontijn, A.; Zellner, R. *Reactions of Small Transient Species*; Fontijn, A., Clyne, M. A. A., Ed.; Academic: London, 1983.
(30) Chantry, P. *J. Chem. Phys.* **1969**, *51*, 3369.
(31) Yarkony, D. *J. Chem. Phys.* **1983**, *78*, 6763.
(32) Cohen, N. *Int. J. Chem. Kinet.* **1989**, *21*, 909.
(33) Costes, M.; Naulin, C.; Moudden, Z.; Dorthe, G. *J. Phys. Chem.* **1991**, *95*, 8244.
(34) Herschbach, D. R. *Adv. Chem. Phys.* **1966**, *10*, 319.
(35) Husain, D. *J. Chem. Soc., Faraday Trans. 2* **1989**, *85* (2), 85.
(36) Nien, C. F.; Plane, J. M. C. *J. Chem. Phys.* **1991**, *94*, 7193.
(37) JANAF Thermochemical Tables. *J. Phys. Chem. Ref. Data* **1985**, *14* (Suppl. 1).